This is the accepted manuscript made available via CHORUS. The article has been published as:

Geometric Phase Appears in the Ultracold Hydrogen Exchange Reaction

B. K. Kendrick, Jisha Hazra, and N. Balakrishnan

Phys. Rev. Lett. **115**, 153201 — Published 8 October 2015

DOI: 10.1103/PhysRevLett.115.153201

Geometric Phase Appears in the Ultracold Hydrogen Exchange Reaction

B. K. Kendrick,[1] Jisha Hazra,[2] and N. Balakrishnan[2]

[1] *Theoretical Division (T-1, MS B221), Los Alamos National Laboratory, Los Alamos, New Mexico 87545, USA**

[2] *Department of Chemistry, University of Nevada, Las Vegas, Nevada 89154, USA*

Abstract

Quantum reactive scattering calculations for the hydrogen exchange reaction H + $H_2(v = 4, j = 0) \rightarrow$ H + $H_2(v', j')$ and its isotopic analogues are reported for ultracold collision energies. Due to the unique properties associated with ultracold collisions, it is shown that the geometric phase effectively controls the reactivity. The rotationally resolved rate coefficients computed with and without the geometric phase are shown to differ by up to four orders of magnitude. The effect is also significant in the vibrationally resolved and total rate coefficients. The dynamical origin of the effect is discussed and the large geometric phase effect reported here might be exploited to control the reactivity through the application of external fields or by the selection of a particular nuclear spin state.

In the Born-Oppenheimer description of molecules the electronic Schrödinger equation is solved to obtain an effective potential energy surface (PES) which is then used in the solution of the nuclear motion Schrödinger equation. The electronic PES often becomes degenerate with an excited electronic state resulting in a conical intersection (CI). As noted long ago by Longuet-Higgins[1] and Herzberg and Longuet-Higgins,[2] the electronic wave functions associated with a CI change sign for any nuclear motion pathway which encircles the CI (i.e., they are double-valued). The electronic sign change implies that a corresponding sign change must also occur on the nuclear motion wave function. Mead and Truhlar[3] showed that this can be accomplished by including an effective vector potential in the nuclear motion Hamiltonian. Mead[4] originally referred to this effect as the "Molecular Aharonov-Bohm" effect but it is now commonly referred to as the "geometric phase" or "Berry's phase" effect.[5, 6]

The most studied of all chemical reactions is the hydrogen exchange reaction H + H_2 $\rightarrow$ H + H_2 and its isotopic analogues H + HD $\leftrightarrow$ D + H_2 and D + HD $\leftrightarrow$ H + D_2.[7–9] The H_3 system exhibits a CI between the ground and first excited electronic states for equilateral triangle (*i.e.*, D_{3h}) geometries.[10] As first predicted by Mead, the GP alters the relative sign between the reactive and non-reactive scattering amplitudes for the H + H_2 reaction which significantly alters the angular dependence of the differential cross sections (DCSs).[11, 12] Unfortunately, state-resolved experiments for H + H_2 are very difficult in practice and Mead's predictions have not yet been verified. Though the isotopic variants are more accessible experimentally, theoretical calculations showed negligible GP effects for a wide range of collision energies.[13–21] Some relatively small rapidly varying oscillations in the DCS due to the GP have been seen in the theoretical DCSs at energies below that of the CI.[17, 22, 23] At energies above the CI, large GP effects on the DCS's were predicted which give rise to broader bi-modal features.[22–24] However, GP effects remained elusive in the integral cross sections or reaction rate coefficients at any energy. A recent experimental attempt to measure the GP oscillations in the DCSs for the H + HD $\rightarrow$ H + HD reaction at energies below the CI was unsuccessful.[25]

Until recently,[26] all previous theoretical predictions of GP effects on chemical reactivity and experimental attempts at its detection have been done at thermal energies. Recent experimental progress in the cooling and trapping of molecules presents a novel energy regime at sub-Kelvin temperatures to explore GP effects in chemical reactions.[27, 28] In the

zero-temperature limit where only s-wave contributes, the reaction rate coefficients obey the well known Bethe-Wigner threshold laws and approach finite measurable values for exoergic processes.[29–33] In this regime, scattering becomes isotropic and for reactions that proceed over a potential well, the scattering phase shifts approach an integral multiple of π. In this Letter, it is shown that these unique properties of ultracold reactions lead to maximal possible interference between the different scattering pathways around a conical intersection. The maximal interference effects are shown to occur in the fundamental hydrogen exchange reaction which results in very large GP effects, essentially turning on or off the reactivity. The effective quantization of the scattering phase shifts is a general property of ultracold collisions for interaction potentials which support bound states[26, 34] as well as those which do not (as demonstrated in this Letter for the H_3 system). In the latter case, suitable vibrational excitation of the reactant diatomic molecule is required which results in an effective reaction pathway (along the vibrational adiabat) that is barrierless[35] and exhibits a potential well.[9, 36–38]

Figure 1 plots a 2D slice of the 3D ground state H_3 electronic PES[39] and reaction pathways for the D + HD $\rightarrow$ D + HD (panel a) and D + HD $\rightarrow$ H + D_2 (panel b) reactions. Hyperspherical coordinates are used which have the advantage of showing all arrangement channels simultaneously as well as the prominent CI located near the center of the plot.[40] Figure 1 corresponds to a stereographic projection of the upper half of the hypersphere with a fixed hyperradius of $\rho = 3.75\,\mathrm{a_o}$. The zero of energy is the bottom of the asymptotic H + D_2 potential well. The contour lines are separated by $2,900\,\mathrm{K}$ except for the two closely spaced contours at $4,640\,\mathrm{K}$ and $5,220\,\mathrm{K}$. For clarity, a cut-plane is used at $33,640\,\mathrm{K}$ so that the extremely repulsive regions for each channel are not included. The energy of the CI in Fig. 1 is $37,700\,\mathrm{K}$ and the PES for the excited electronic state is not shown.

The two panels in Figure 1 depict the interference pathways which can lead to significant GP effects for each reaction. In general the total scattering amplitude can be decomposed into contributions from each pathway labeled by the 1, 2, and 3 in panels (a) and (b).[11, 18–20] For the inelastic scattering in 1 (a), pathway #1 (black) corresponds to a non-reactive process and pathways #2 and #3 (red) correspond to an exchange process where the two identical D nuclei in each HD channel are exchanged. For the reactive scattering in 1 (b), pathway #1 (black) corresponds to a direct reaction process and pathway #2 (red) corresponds to a looping reaction process. For the D-atom exchange in 1 (a), it has been

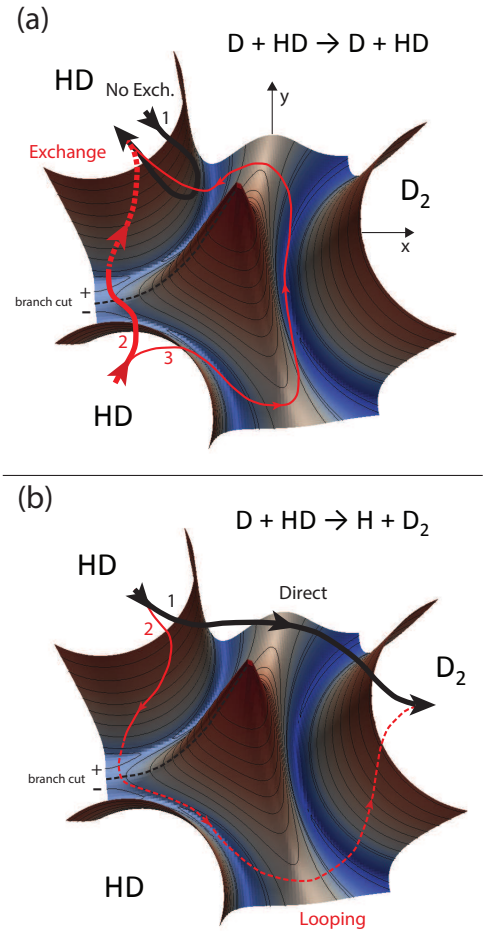

FIG. 1. (color online) A 2D slice of the 3D Born-Oppenheimer PES for the HD_2 system is plotted at a fixed hyperradius $\rho = 3.75\,a_o$. The different scattering pathways around the CI are indicated, panel (a) for D + HD → D + HD, and panel (b) for D + HD → H + D_2. For clarity, pathways for only one of the symmetric HD channels is depicted.

shown that, due to the direct collinear nature of the reaction, contributions from pathway #3 (thin red curve) are negligible even for high collision energies approaching that of the CI.[13–18] Thus, the total scattering amplitude which does not include the GP can be written as $\tilde{f}^{\rm NGP} = (1/\sqrt{2})(\tilde{f}_1 + \tilde{f}_2)$ where NGP denotes "No Geometric Phase" and $\tilde{f}_1$ and $\tilde{f}_2$ are the scattering amplitudes for pathways #1 and #2 in Fig. 1 (a).[11, 18–20] The GP alters the sign on the scattering amplitude for pathway #2 across the branch cut (black dashed curve in Fig. 1). Thus, the total scattering amplitude which includes the GP is given by $\tilde{f}^{\rm GP} = (1/\sqrt{2})(\tilde{f}_1 - \tilde{f}_2)$ where GP denotes "with Geometric Phase".[11, 18–20] The same expressions hold for the NGP and GP scattering amplitudes in Fig. 1 (b).[18–20] The

encirclement of the CI by the combined pathways #1 and #2 is obvious in Fig. 1 (b) but not so obvious in Fig. 1 (a). Pathway #2 in Fig. 1 (a) encircles the CI through "symmetric encirclement" (i.e., via the symmetrization of the wave function with respect to permutation of the identical D nuclei).[3, 11, 18–20, 41]

The cross sections and rate coefficients are computed from the square modulus of the total scattering amplitude $||\tilde{f}|| = (1/2)\,(f_1^2 + f_2^2 \pm 2\,f_1\,f_2\,\cos\Delta)$ where the + and − denote NGP and GP, respectively. The complex scattering amplitudes are expressed as $\tilde{f}_1 = f_1 \exp(i\,\delta_1)$, $\tilde{f}_2 = f_2 \exp(i\,\delta_2)$ and the phase difference $\Delta = \delta_2 - \delta_1$. If the square modulus of the scattering amplitude for one of the pathways is much larger than the other: $f_1^2 >> f_2^2$ or $f_2^2 >> f_1^2$, then the square modulus of the total scattering amplitude is given by $||\tilde{f}|| \approx f_1^2/2$ or $||\tilde{f}|| \approx f_2^2/2$, respectively, and the GP effect is negligible. However, when the squared moduli are similar $f_1^2 \approx f_2^2$, then $||\tilde{f}|| \approx f^2\,(1 \pm \cos\Delta)$ where $f = f_1 \approx f_2$. Thus, depending upon the sign and magnitude of $\cos\Delta$, the reactivity can be dramatically enhanced or suppressed. The maximum interference occurs when $|\cos\Delta| = 1$. If $\pm\cos\Delta = +1$ then maximum constructive interference occurs and $||\tilde{f}|| \approx 2\,f^2$, whereas for $\pm\cos\Delta = -1$, maximum destructive interference occurs and $||\tilde{f}|| \approx 0$. That is, if $|\cos\Delta| \approx 1$ then the reactivity can be turned on or off by the sign of the interference term. Since the GP alters the sign of the interference term, the GP effectively controls the reactivity.

The quantum reactive scattering calculations for the H_3 system were done using a numerically exact time-independent coupled-channel method based on hyperspherical coordinates and the GP effect is included using the vector potential approach.[16, 34, 40, 42–44] We note that the GP effect is accounted for if non-adiabatic couplings to excited electronic states are included. However, this would require a 2×2 diabatic matrix representation[45] of the interaction potential with an associated $2^3 = 8$ fold increase in computational cost. The computed scattering (S) matrices include all open reactant and product diatomic vibrational and rotational states on a grid consisting of 71 collision energies spanning the range from $1\,\mu$K to 100 K relative to asymptotic energy of HD($v = 4$, $j = 0$) for the H + HD and D + HD reactions, and H_2($v = 4$, $j = 0$) for H + H_2. The 21 collision energies below 0.1 K are logarithmically spaced while the remaining 50 higher-lying energies are uniformly spaced. For the highly excited reactant vibrational states, the reaction becomes effectively barrierless and exhibits significant reactivity at ultracold collision energies.[35] The asymptotic energies for HD($v = 4$, $j = 0$) and H_2($v = 4$, $j = 0$) are 22,109 K and 25,078 K relative to

the bottom of the asymptotic diatomic potential wells, respectively. The scattering calculations were carried out using two accurate *ab initio* electronic PESs for the H_3 system: the BKMP2[39] and the newer one by Mielke, et al.[46] which includes significant improvements to the long-range anisotropic behavior.

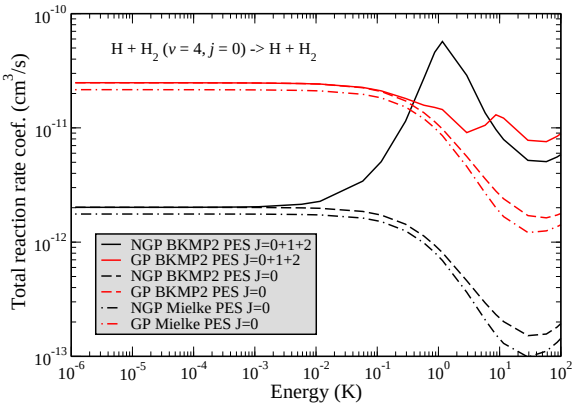

FIG. 2. (color online) The total reaction rate coefficient for the H + $H_2(v = 4, j = 0) \rightarrow$ H + H_2 (para-para) reaction is plotted as a function of collision energy. The solid curves include all values of total angular momentum $J = 0 - 2$. The dashed and long-short dashed curves include only $J = 0$ and were done using the BKMP2 and Mielke PESs, respectively. The red curves include the geometric phase (GP) while the black curves do not (NGP).

Figure 2 plots the total reaction rate coefficient for H + $H_2(v = 4, j = 0) \rightarrow$ H + H_2 summed over all product vibrational and even rotational states (i.e., the para-para transitions). The results which include (do not include) the GP are plotted in red (black). The solid curves include all values of total angular momentum (i.e., orbital l plus rotational j) $J = 0 - 2$ and the dashed and long-short dashed curves are for $J = 0$ only (for which $l = j = 0$). The rate coefficients for each value of J are well converged over the entire energy range. The total rate coefficient is well converged with respect to the sum over $J = 0 - 2$ up to about 2 K.[34] The dashed and long-short dashed curves compare the results based on the BKMP2 and Mielke PES, respectively. Both PESs give similar results and predict that the GP enhances the ultracold reactivity by a full order of magnitude. Figure 3 plots several representative rate coefficients for the D + HD($v = 4$, $j = 0$) $\rightarrow$ D + HD(v', j') reaction using the BKMP2 PES. The rate coefficients are computed for even exchange symmetry (i.e., the nuclear motion wave function is symmetric with respect to permutation of

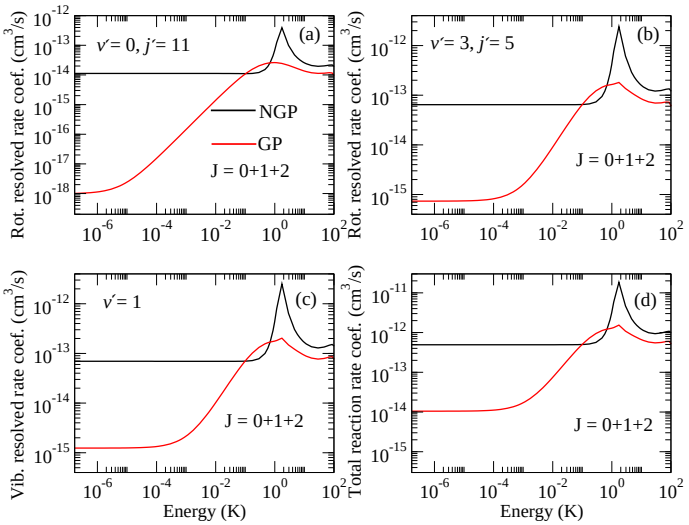

FIG. 3. (color online) Reaction rate coefficients for the D + HD($v = 4$, $j = 0$) → D + HD(v', j') reaction are plotted as a function of collision energy: (a) $v' = 0$, $j' = 11$, (b) $v' = 3$, $j' = 5$, (c) $v' = 1$, and (d) total. The results are for even exchange symmetry, include all values of total angular momentum $J = 0 - 2$, and are based on the BKMP2 PES. The red curves include the geometric phase (GP) while the black curves do not (NGP).

the identical D nuclei) and include all values of total angular momentum $J = 0 - 2$. The rotationally resolved rate coefficient for $v' = 0$, $j' = 11$ shows that the geometric phase reduces the reactivity by over four orders of magnitude. The rate coefficient for $v' = 3$, $j' = 5$ and the vibrationally resolved rate coefficient for $v' = 1$ are reduced by nearly two orders of magnitude when the GP is included. The total rate coefficient which includes the GP is reduced by a factor of 50. The rate coefficients for odd exchange symmetry are similar in magnitude except that the GP increases the reactivity in this case.[34] When both the symmetric and antisymmetric nuclear spin states of D_2 are present, the scattering results must be summed over both even and odd exchange symmetries including the appropriate nuclear spin statistical weights 2/3 and 1/3, respectively. The GP effect is reduced but remains significant (see Table I and Ref. 34). We have also verified large GP effects for other reactant vibrational states, in particular $v = 3$ and $v = 5$. A notable feature in Figs. 2 and 3 is the bump which occurs near 1 K. This feature is most likely a shape resonance due to the centrifugal barrier for $J > 0$.[31, 34]

Table I lists a representative sample of the ultracold (1μK) reaction rate coefficients com-

puted for the H_3 system both with and without the geometric phase and different exchange symmetries. Most notable are the very large GP effects seen in the rotationally resolved rate coefficients for the D + HD $\rightarrow$ D + HD reaction for each exchange symmetry. These differences persist, albeit smaller when summed over both exchange symmetries. The GP effects for the H + HD $\rightarrow$ H + HD reaction are overall smaller than those for the D + HD reaction. For the H + H_2 $\rightarrow$ H + H_2 para-para reaction, the results have already been summed over the appropriate nuclear spin states. Large differences ($\approx$ 10x) between the GP and NGP rate coefficients are observed even when summed over all v' and j'. The total rate coefficients summed over all v' and j' using the PES of Mielke et al. are tabulated in the last column. They are very similar at the state resolved level as well but the overall reactivity is slightly reduced (see Fig. 2). For the D + HD $\rightarrow$ H + D_2 and H + HD $\rightarrow$ D + H_2 reactions (not tabulated), the GP and NGP rate coefficients are nearly identical even at the rotationally resolved and single exchange symmetry level. The same applies to the H + H_2 para-ortho reaction (not tabulated). The lack of GP effects for these ultracold reactions is due to the direct collinear nature of the reaction which results in a tiny contribution from the scattering amplitude corresponding to looping pathway in Fig. 1 (b).

For ultracold collisions of H or D with a high vibrationally excited HD or H_2 diatomic molecule, leading to vibrational quenching, the reaction pathway is effectively barrierless with an attractive potential well.[9, 35–38] Thus, each scattering pathway in Fig. 1 can be represented by a simple 1D spherical well model. For this 1D model, the scattering phase shifts are known analytically and in the zero energy limit they become effectively quantized (i.e., they approach $n\,\pi$ where n denotes the number of bound states in 1D spherical well).[26, 34] If the number of bound states in the two different 1D spherical well potentials corresponding to the two reaction pathways in Fig. 1(a) differ by an even (odd) number, then $\cos\Delta = 1$ ($\cos\Delta = -1$). Maximum constructive (destructive) interference will occur between the two scattering amplitudes contributing to $\tilde{f}^{\rm NGP}$, and the opposite interference behavior will occur for $\tilde{f}^{\rm GP}$. Thus, the unusually large GP effects reported here originate from the isotropic (s-wave) scattering and the effective quantization of the scattering phase shift which results in $|\cos\Delta| \approx 1$.[26, 34] The mechanism is general and is expected to hold for many molecules which exhibit CIs and for which the PES and/or the choice of reactant and product states allows for a favorable encirclement.[26]

We emphasize that the interference mechanism reported here is a general property of

TABLE I. Ultracold (1 μK) reaction rate coefficients for the X + HD($v = 4$, $j = 0$) $\rightarrow$ X + HD(v', j') with X=D and H, and the H + H_2($v = 4$, $j = 0$) $\rightarrow$ H + H_2(v', j' even) reactions. The "evn" and "odd" denote exchange symmetry and the "GP" and "NGP" denote the results computed with and without the geometric phase, respectively. The "(evn) + (odd)" denote the summed results over even and odd exchange symmetries. All rate coefficients include the appropriate nuclear spin statistical weights and are in cm^3/s. Data correspond to the BKMP2 PES, except for the last column which is obtained on the PES of Mielke et al.

Reaction		v'=0,j'=11	v'=2,$\sum_{j'}$	Total	Mielke PES
D + HD(evn)	GP	1.01(-18)	1.51(-15)	1.05(-14)	6.64(-15)
	NGP	1.13(-14)	1.52(-13)	4.94(-13)	2.51(-13)
D + HD(odd)	GP	5.48(-15)	7.52(-14)	2.44(-13)	1.25(-13)
	NGP	1.90(-19)	7.42(-16)	4.99(-15)	2.97(-15)
(evn) + (odd)	GP	5.48(-15)	7.67(-14)	2.54(-13)	1.32(-13)
	NGP	1.13(-14)	1.53(-13)	4.98(-13)	2.54(-13)
		v'=0,j'=2	v'=0,$\sum_{j'}$		
H + HD(evn)	GP	1.60(-17)	1.58(-14)	9.87(-14)	
	NGP	1.22(-14)	8.80(-14)	3.15(-13)	
H + HD(odd)	GP	3.79(-14)	2.71(-13)	9.35(-13)	
	NGP	1.95(-17)	4.34(-14)	2.85(-13)	
(evn) + (odd)	GP	3.79(-14)	2.87(-13)	1.03(-12)	
	NGP	1.22(-14)	1.31(-13)	6.00(-13)	
		v'=3,j'=4	v'=3,$\sum_{j'}$		
H + H_2	GP	4.32(-11)	8.39(-12)	2.48(-11)	2.16(-11)
	NGP	2.16(-13)	5.41(-13)	2.02(-12)	1.76(-12)

ultracold collisions and will also occur in molecules without CIs or GP effects. In general, large interference effects can be expected for barrierless reaction paths which proceed over a potential well (due to the PES or vibrational excitation) and include contributions from two interfering pathways (such as reactive and non-reactive). Experimentally the interference (and hence reactivity) might be controlled by the selection of a specific nuclear spin state or by the application of external electric or magnetic fields to (1) alter the relative number

of bound states in the effective potential wells along each interfering pathway, or (2) alter the relative magnitude of the two interfering scattering amplitudes.[26, 47]

Acknowledgments

BKK acknowledges that part of this work was done under the auspices of the US Department of Energy under Project No. 20140309ER of the Laboratory Directed Research and Development Program at Los Alamos National Laboratory. Los Alamos National Laboratory is operated by Los Alamos National Security, LLC, for the National Security Administration of the US Department of Energy under contract DE-AC52-06NA25396. The UNLV team acknowledges support from the Army Research Office, MURI grant No. W911NF-12-1-0476 and the National Science Foundation, grant Nos. PHY-1205838 and PHY-1505557.

---

* Correspondence should be addressed to BKK (bkendric@lanl.gov).

1. H. C. Longuet-Higgins, U. Öpik, M. H. L. Pryce, and R. A. Sack, *Proc. R. Soc. London, Ser. A* **244**, 1 (1958).
2. G. Herzberg and H. C. Longuet-Higgins, *Discuss. Faraday Soc.* **35**, 77 (1963).
3. C. A. Mead and D. G. Truhlar, *J. Chem. Phys.* **70**, 2284 (1979); **78**, 6344E (1983).
4. C. A. Mead, *Chem. Phys.* **49**, 23 (1980).
5. M. V. Berry, *Proc. R. Soc. London Ser. A* **392**, 45 (1984).
6. A. Bohm, *Quantum Mechanics: Foundations and Applications*, 3rd Edition, (Springer-Verlag, New York), Chapters XII and XIII, (1993), (2001).
7. D. G. Truhlar and R. E. Wyatt, *Ann. Rev. Phys. Chem.* **27**, 1 (1976).
8. S. L. Mielke, et al., *Phys. Rev. Lett* **91**, 063201-1 (2003).
9. J. Jankunas, M. Sneha, R. N. Zare, F. Bouakline, S. C. Althorpe, D. Herráez-Aguilar, and F. J. Aoiz, *PNAS* **111**, 15 (2014).
10. A. J. C. Varandas, F. B. Brown, C. A. Mead and D. G. Truhlar, *J. Chem. Phys.* **86**, 6258 (1987).
11. C. A. Mead, *J. Chem. Phys.* **72**, 3839 (1980.)
12. B. Lepetit, A. Kuppermann, *Chem. Phys, Lett.* **166**, 581 (1990).
13. B. K. Kendrick, *J. Chem. Phys.* **112**, 5679 (2000); **114**, 4335E (2001).

14. B. K. Kendrick, *J. Chem. Phys.* **1**14, 8796 (2001).
15. B. K. Kendrick, *J. Chem. Phys.* **1**18, 10502 (2003).
16. B. K. Kendrick, *J. Phys. Chem.* **107**, 6739, (2003).
17. C. Juanes-Marcos, S. C. Althorpe, *J. Chem. Phys.* **122**, 204324 (2005).
18. J. C. Juanes-Marcos, S. C. Althorpe and E. Wrede, *Science* **309**, 1227 (2005).
19. S. C. Althorpe, *J. Chem. Phys.* **124**, 084105 (2006).
20. S. C. Althorpe, T. Stecher, and F. Bouakline, *J. Chem. Phys.* **129**, 214117 (2008).
21. F. Bouakline, *Chem. Phys.* **442**, 31-40 (2014).
22. F. Bouakline, B. Lepetit, S. C. Althorpe, and A. Kuppermann, in "The Jahn-Teller effect fundamentals and implications for physics and chemistry", Castleman, Jr., A. P., Toennies, J. P., Yamanouchi, K., & Zinth, W. Eds. *Springer Series in Chemical Physics*, **9**7, 201-237 (2009).
23. F. Bouakline, S. C. Althorpe, and D. P. Ruiz, *J. Chem. Phys.* **1**28, 124322 (2008).
24. F. Bouakline, S. C. Althorpe, P. Larregaray, and L. Bonnet, *Molec. Phys.* **108**, 969-980 (2010).
25. J. Jankunas, M. Sneha, R. N. Zare, F. Bouakline, and S. C. Althorpe, *J. Chem. Phys.* **139**, 144316 (2013).
26. B. K. Kendrick, J. Hazra and N. Balakrishnan, *Nat. Commun.* 6:7918 doi: 10.1038/ncomms8918 (2015).
27. L. D. Carr, D. DeMille, R. V. Krems, J. Ye, New. J. Phys. **11**, 055049 (2009).
28. S. Ospelkaus *et al.*, Science **327**, 853 (2010).
29. H. A. Bethe, *Phys. Rev.* **47**, 747 (1935).
30. E. P. Wigner, *Phys. Rev.* **73**, 1002 (1948).
31. D. W. Schwenke and D. G. Truhlar, *J. Chem. Phys.* **83**, 3454 (1985).
32. W. C. Stwalley, *Can. J. Chem.* **82**, 709 (2004).
33. P. F. Weck and N. Balakrishnan, *Int. Rev. Phys. Chem.*, **25**, 283 (2006).
34. See the online supplementary material for more details.
35. I. Simbotin, S. Ghosal, and R. Côté, *Phys. Chem. Chem. Phys.* **13**, 19148 (2011).
36. D. G. Truhlar, *J. Chem. Phys.* **53**, 2041 (1970).
37. W. H. Miller, N. C. Handy, and J. E. Adams, *J. Chem. Phys.* **72**, 99 (1980).
38. D. G. Truhlar, B. C. Garrett, and J. S. Klippenstein, *J. Phys. Chem.* **100**, 12771 (1996).
39. A. I. Boothroyd, W. J. Keogh, P. G. Martin, and M. R. Peterson, *J. Chem. Phys.* **104**, 7139

(1996).

40. R. T Pack, G. A. Parker, *J. Chem. Phys.* **87**, 3888 (1987).
41. B. Kendrick and C. A. Mead, *J. Chem. Phys.* **102**, 4160 (1995).
42. B. Kendrick and R. T Pack, *J. Chem. Phys.* **1**04, 7475 (1996).
43. B. K. Kendrick, R. T Pack, R. B. Walker and E. F. Hayes, *J. Chem. Phys.* **110**, 6673 (1999).
44. C. Makrides *et al.*, *Phys. Rev. A* **91**, 012708 (2015).
45. C. A. Mead, *J. Chem. Phys.* **78**, 807 (1983).
46. S. L. Mielke, B. C. Garrett, and K. A. Peterson, *J. Chem. Phys.* **116**, 4142 (2002).
47. J. Hazra, B. K. Kendrick, N. Balakrishnan, *J. Phys. Chem. A*, doi: 10.1021/acs.jpca.5b06410 (2015).